Photoconductivity and Characterization of Nitrogen Incorporated Hydrogenated Amorphous Carbon Thin Films

Neeraj Dwivedi[a,b], Sushil Kumar[a,*], J. D. Carey[c], Hitendra K. Malik[b] and Govind[a]

[a] *National Physical Laboratory (CSIR), K.S. Krishnan Road, New Delhi – 110 012, India,*

[b] *Department of Physics, Indian Institute of Technology Delhi, New Delhi-110016, India,*

[c] *Advanced Technology Institute, University of Surrey, Guildford GU2 7XH, United Kingdom*

ABSTRACT

The observation and origin of photoconductivity in high base pressure (~10^{-3} Torr) grown nitrogen incorporated hydrogenated amorphous carbon (a-C:H:N) thin films is reported. The magnitude of conductivity at room temperature was measured to increase by nearly two orders of magnitude and exhibits a maximum ratio of photoconductivity to dark conductivity of 1.5 as the nitrogen content increased to 15.1 at.%. X-ray photoelectron spectroscopy (XPS), micro-Raman spectroscopy and Fourier transform infrared (FTIR) spectroscopy reveal enhanced sp^2 bonding at higher nitrogen contents. Residual film stress, Tauc band gap, hardness and elastic modulus are all found to decrease with addition of nitrogen. The electrical characteristics suggest the creation of a-C:H:N/p-Si heterojunction diodes having rectifying behavior. The conductivity and electrical characteristics are discussed in term of band model and the results show that high quality a-C:H:N films can be grown at high base pressures with properties comparable to those grown at low base pressures.

*Corresponding Author. Tel.: +91 11 45608650; Fax: +91 11 45609310.
E-mail address: skumar@nplindia.org (Sushil Kumar)

I. INTRODUCTION

Owing to their remarkable mechanical properties, hard hydrogenated amorphous carbon (a-C:H) and unhydrogenated amorphous carbon (a-C), also called diamond-like carbon (DLC), thin films have attracted considerable attention. Along with the introduction of nitrogen, the resultant nitrogenated a-C:H (a-C:H:N) and a-C (a-C:N) thin films have shown the great promise with properties[1] approaching that β-C_3N_4, whose characteristics, such as hardness, have been found to be comparable to that of superhard diamond. Not only are the mechanical properties of a-C:H films of interest but also the electrical and optical properties have also been explored. Silva *et al.*[2], Schwan *et al.*[3] and Godet *et al.*[4] have explored the electrical properties of a-C:H:N films and have suggested models which help to explain electron transport. Recently, we[5,6] have investigated some of the electrical properties of a-C:H:N and Ti/DLC multilayer films. For a-C:H:N films on a Si substrate we have shown the formation of a heterojunction along with improved electrical characteristics.[5] The thin Ti layers present in the Ti/DLC multilayer structure help to promote nanostructured DLC film with sphere- and rod-like structures, which further give rise to enhance conductivity.[6] If we look at the optoelectronic applications, c-Si/a-C:H hetero- and a-C/a-C homojunction solar cells have been fabricated[7,8], though the understanding of the photoconduction mechanism remains to be resolved. Nonetheless, Konofaos *et al.*[9] and Gao *et al.*[10] have demonstrated the formation of diamond-like carbon/silicon heterojunction devices. Lazar *et al.*[11] have developed a-C:H based metal-insulator-metal (MIM) and metal-insulator-semiconductor (MIS) structures and observed space charge limited conduction in their devices. While various other conduction mechanisms, which includes band tail hopping have also been reported[2-4] in films grown at low pressure, it remains important to understand the physics related to the conduction in a-C:H and modified a-C:H films especially those grown at high pressures.

A-C:H thin films are disordered semiconductors, in which the conduction and valence bands are not sharp. Such semiconductors show partially localized states near the Fermi level and in the band tails in addition to their extended states at higher energies. A-C:H films contain π and π* states, associated predominantly with sp^2 bonding, which lie inside the σ and σ* states, associated with sp^3 bonding. The electrical, optical and optoelectronic properties of these films are governed by sp^2 bonding, whereas sp^3 bonding maintains the mechanical properties.[12] The activation energy for conduction, estimated from electrical measurements, is an important parameter in determining the electron transport through disorder semiconductors. Silva *et al.*[2] have suggested that a shifting of E_F with the nitrogen introduction can be a cause of changes in the activation energy. However, Ronning *et al.*[13] have argued that nitrogen introduction increases the states, which changes the activation energy as well as conductivity. On the other hand, Godet *et al.*[4, 14] have suggested that nitrogen introduction causes a reduction of concentration of states and this governs the conduction mechanism.

Although a-C:H and modified a-C:H films have been studied previously, the following issues need to be explored systematically in order to enhance their scientific and industrial impact:

(1) Photoconductivity (PC) in a-C:H films may be possible when there are electron-hole excitations between π-π* states. It is well known that a-C:H is generally a poor photoconducting material, since the photo-generated charge carriers have low mobility, are bound together and tend to recombine leading to a high photoluminescence efficiency.[3,15]

(2) The a-C:H films exhibit high residual stress that leads to early delamination of the films from the substrate. For example, Schwan *et al.*[3] have observed very high stress, which varied from 6 - 12 GPa in a-C:H films.

(3) The third issue is related to throughput and the cost. Usually a-C:H films are deposited at low base pressure (10^{-5} Torr or less), which requires sufficient pumping time and expensive

vacuum equipment. For industrial applications the process should be simple, throughput should be high and ultimately the product cost should be low. It is this final issue that lies at the core of this study where a higher base pressure is used in the deposition of the films.

Nitrogen has proved to be an important foreign element for a-C:H films that can help solve the first two problems mentioned above. Low residual stress in nitrogenated a-C:H (a-C:H:N) films, in which the residual stress is decreased from 4.6 GPa to 1.5 GPa with the increasing nitrogen partial pressure from 0% to ~ 60%, have been prepared previously.[16] Silva *et al.*[2] have also observed decrease in residual stress from ~ 5 GPa to 1 GPa with the increasing nitrogen content from 0 at.% to ~ 15 at.%. Dwivedi *et al.*[5] and Kumar *et al.*[16] have realized the improved electrical and optical characteristics at low base pressure (10^{-5} Torr and less) deposited a-C:H:N films due to nitrogen incorporation. The cost effective a-C:H:N films can be deposited, without an use of turbo molecular pump, at a higher base pressure and offers advantages in terms of cost and speed of production. In the present study, higher base pressure (~ 10^{-3} Torr) deposited a-C:H:N films are studied for their electrical, optical, mechanical and structural properties. The photoconductivity (PC), dark conductivity (DC), activation energy, Tauc band gap, current-voltage (I-V) characteristics, hardness, residual stress are evaluated and correlated with the structure and the bonding environment within the films.

II. EXPERIMENTAL DETAILS

Nitrogen incorporated hydrogenated amorphous carbon (a-C:H:N) films were deposited on cleaned corning 7059 glass and p-type Si <100> wafers using asymmetric capacitive coupled radio frequency 13.56 MHz plasma enhanced chemical vapor deposition (RF-PECVD). Besides standard three stage solvent cleaning, the substrates were also cleaned in an Ar plasma for 10 minutes prior to the deposition of films. Four sets of a-C:H:N films were deposited at different

nitrogen partial pressure (NPP) of 0% (S-1), 44.4% (S-2), 66.6% (S-3) and 76.1% (S-4), respectively, whereas all other process parameters, such as a negative self-bias of 100 V, were kept constant.

The thickness of the films was measured using a Taylor-Hobson Talystep instrument and found to be 276 nm, 244 nm, 195 nm and 162 nm in samples S-1, S-2, S-3 and S-4, respectively. Keithley solid state electrometer (610C) was used to measure both the DC and PC. The PC was evaluated by exposing the samples to a photon power density of 100 mW/cm^2, where the samples were metalized into coplanar structures. The surface composition and the bonding of the films was investigated by X-ray photoelectron spectroscopy (XPS) (Perkin Elmer, USA, model no. 1257) and time-of-flight secondary ion mass spectroscopy (TOF-SIMS) (ION-TOF GmBH, Germany) was used to analyze the bulk composition and depth profile of the films. Micro-Raman measurements were carried out on these films using a Renishaw inVia reflex micro-Raman spectrometer employing an excitation wavelength of 514.5 nm. Fourier transform infrared (FTIR) spectroscopy (model Perkin Elmer spectrum BX) analysis was performed to investigate the bonding environment. The optical measurements were performed using Schimadzu ultra-violet (UV-Vis) spectrometer for determination of the Tauc band gap (E_g). In order to evaluate E_g, first the absorption coefficient (α) was estimated using the relation $\alpha = 1 / d\ [\ln \{(1-R) / T\}]$, where d, R and T are the thickness, reflection and transmission, respectively. A (Tauc) plot $(\alpha h\nu)^{1/2}$ versus hν gives the values of E_g. The residual stress (S) in these films was measured using 500TC temperature controlled film stress measurement system (FSM Frontier Semiconductor, USA). We calculated the residual stress using Stoney formula, as

$$S= \frac{E_s {d_s}^2}{6(1-\nu_s)d_f}\left(\frac{1}{R_f}-\frac{1}{R_0}\right) \quad (1)$$

where E_s, ν_s, d_f and d_s are Young's modulus, Poisson ratio, thickness of film and thickness of substrate, respectively, and R_0 and R_f are the radii of substrate curvature before and after film deposition. Fully automatic software controlled IBIS nanoindentation (Fisher-Cripps laboratories Pvt. Limited, Australia) with a diamond Berkovich indenter at indentation load of 10 mN was employed to measure the nano-mechanical properties of the a-C:H:N films.

III. RESULTS AND DISCUSSION

A. XPS analysis

XPS is an important technique for investigation of surface composition and chemical analysis. The XPS spectra in the binding energy range of 200 - 600 eV for a-C:H:N films deposited at NPPs of 0% (S-1) and 76.1% (S-4) reveal the presence of C and O atoms. The presence of nitrogen atoms is only observed in sample S-4. Figure 1(a)-1(c) show the XPS core level spectra of C1s and N1s for different a-C:H:N films. The nitrogen content of sample S-4 was estimated using the ratio of area of peaks obtained from the N1s and C1s core level spectra i.e. $N/(N+C) = (A_N / 0.38) / (A_N / 0.38 + A_C / 0.205)$, where A_N and A_C are the areas under the N1s and C1s core level spectra and the constants 0.38 and 0.205 are the atomic sensitivity factors of nitrogen and carbon, respectively.[17] The amount of nitrogen in sample S-4 was found to be 15.1 at.%. The core level spectra were deconvolved to examine the bonding states of C with C, N and O; Figure 1a shows the deconvolved C1s core level spectra of sample S-1. The peaks centered at 284.1 eV and 285.1 eV represent the sp^2 and sp^3 hybridized carbon-carbon bonding. The peak located at 286.3 eV shows the bonding state of carbon with oxygen. During the peak fitting, the full width at half maximum (FWHM) values of these peaks was kept at 1.67, 1.6 and 2.0 eV, respectively. Similarly, the deconvolved C1s core level spectrum of sample S-4 was fitted with four peaks as shown in Fig. 1b. A low intense peak centered at 284.2 eV is generally labeled as adventitious

carbon due to atmospheric contamination and peaks located at the positions of 285.4 eV and 286.5 eV represent the sp^2 and sp^3 hybridized carbon-nitrogen bondings. The low intensity peak centered at 287.6 eV shows evidence of N-O or C-O bondings. The deconvolved N1s core level spectrum of sample S-4 is shown in Fig.1c. This spectrum was fitted with three peaks located at 398.3 eV (C=N–C bonding), 399.6 eV (sp^3 carbon-nitrogen bonding) and 401.2 eV (sp^2 carbon-nitrogen bonding), respectively. For sample S-4, the peaks centered at 284.2 eV and 285.4 eV in C1s spectra are found to be analogous to that of the peak centered at 401.2 eV and 399.6 eV in N1s spectra, which show the carbon-nitrogen bonding in sp^2 and sp^3 hybridization, respectively. By XPS analysis it is confirmed that introduction of nitrogen in a-C:H:N films enhances the graphite-like sp^2 bonding.

B. ToF-SIMS and Deposition Rate Analyses

Since XPS is surface sensitive technique, ToF-SIMS measurement was performed to analyze the bulk composition. SIMS also provides information about film/substrate interface and depth profile of the elements. Typical ToF-SIMS depth profiles for C, H, N, O and Si from a-C:H:N film deposited at NPP of 76.1% (sample S-4) are shown in Fig. 2. It is evident from the figure that C, H and N atoms are present with the incorporation of O as an impurity in the film. It is generally realized that during the growth of pure a-C and a-C:H films, the C ions strike the substrate with high energy and some of them diffuse into the substrate. This may lead to the formation of mixed a-SiC and a-SiC:H kind of layers at the interface. However, compared with a-C:H films[6], the ToF-SIMS depth profile of a-C:H:N film deposited at a NPP of 76.1% reveals negligible interdiffusion of C into the Si substrate. Thus, it is realized that a high NPP restricts the interdiffusion of C into Si. By contrast, H is significantly diffused into the substrate Si due to its low atomic weight. A small amount of O was found in the a-C:H:N film due to atmospheric contamination. It is to be

noted that O is present during the depth profiling of substrate Si, which may be due to the fact that Czochralski technique based Si wafers possess O as an impurity.

The deposition rate of a-C:H:N films was also determined and found to vary inversely with NPP. When NPP (nitrogen content) was increased from 0% to 76.1% (0 at.% to 15.1 at.%) deposition rate decreased from 42 nm/min to 25 nm/min. During growth of a-C:H:N films, there is a competition between growth and etching due to ionic bombardment. An increase in the NPP enhances the nitrogen species in carbon-nitrogen plasma, which further increases the ionic bombardment. This results in more etching of the growing surface and hence, a lower deposition rate.

C. Micro-Raman Spectroscopic and FTIR Analyses

Raman spectroscopy is a powerful non-destructive tool for investigating the bonding in carbon based materials. The excitation wavelength of 514.5 nm (energy ~ 2.4 eV) is used here for micro-Raman measurements, which can only probe directly the sp^2 phase of a-C:H:N films. The Raman spectra of a-C:H and a-C:H:N films exhibit two main features; the D peak (~ 1350 cm^{-1}) and G peak (~ 1550 cm^{-1}). Here D stands for a disorder attributed peak due to breathing modes of six fold sp^2 aromatic clusters. The G peaks arises from vibrations between in sp^2 carbon atoms. Ferrari and Robertson[18] have discussed the origin of the D peak and have suggested that the visible Raman spectra of amorphous carbon films depend on bond length and bond angle disorder, sp^2 rings or chains and the sp^3/sp^2 ratio. Hence, because of variations of the G peak position and the I_D/I_G intensity ratio, change in the sp^2 phase can be probed. Figure 3a and 3b show the Raman spectra of samples S-1 and S-4. The spectra clearly reveal the shifting of G band towards higher wavenumber with an increase in NPP from 0% to 76.1%, which is due to an enhancement in the π-π^* sp^2 bonding. The Raman spectra of these films are fitted with two Gaussian functions in order

to investigate how the I_D/I_G ratio and the G peak position change by varying the NPP. For sample S-1, the G peak is found at 1536 cm^{-1} which shifts to 1548 cm^{-1} in sample S-4 upon nitrogen incorporation. This Raman shift of ~12 cm^{-1} towards higher wavenumber indicates nitrogen driven enhancement of sp^2 bonding. In addition nitrogen incorporation in a-C:H:N film makes the intensity of the D peak higher due to an enhancement in disorder resulting from substitution of N atoms in aromatic sp^2 clusters. This explains why the I_D/I_G ratio increases from 0.31 to 0.48 with the increasing NPP from 0% to 76.1%.

The Fourier transform infrared (FTIR) spectra of samples S-1 and S-4 are shown in Figs. 4a and 4b, respectively. A strong CO_2 peak due to atmospheric contamination was observed in these films; since this peak has no physical significance in relation to the properties of interest, the region 2230 - 2410 cm^{-1} has been removed from the FTIR spectra. The FTIR spectra from sample S-1 shows the presence of sp^n C-H_x (where n = 2, 3 and x = 1, 2 and 3) stretching modes in the range from 2800 - 3100 cm^{-1}. The band in the range 1560 - 1660 cm^{-1} reveals the presence of C=C bonding only. When the NPP (nitrogen content) was increased to 76.1% (15.1 at.%) the band in the range 1560 - 1660 cm^{-1} becomes stronger with a sharp peak at ~ 1600 cm^{-1}. This is attributed to increased sp^2 phase due to C=N bonding (amino group).

D. Residual Stress, Hardness and Elastic Modulus Analyses

The presence of residual stress (S) is a major issue in a-C:H films and excess stress leads to delamination of the films from the substrate. High values of stress restricts the growth of comparatively thick a-C:H films and limits its use in industrial applications. Nitrogen incorporation in a-C:H films has, however, evolved as an important way to reduce excessive stress. The values of S in a-C:H:N films were measured to be in the range between 0.8 GPa and 1.9 GPa (Fig. 5a) and scale inversely with nitrogen partial pressure. In addition, Figure 5b and 5c

show the variation of hardness (*H*) and elastic modulus (E), respectively with NPP for different a-C:H:N films. The values of *H* and E in these films were found to be significantly high and varied in the range 38 - 22 GPa and 462 - 330 GPa, respectively with the increasing nitrogen content. The observed reduction in S and *H* with an enhancement in NPP was due to the increased sp^2 bonding. Such a-C:H:N films with high value of *H* may be useful for their hard, protective, encapsulate and anti-reflection coating on silicon solar cells.

E. Tauc Band Gap Analysis

Figure 6 shows the variation of the Tauc band gap (E_g) with nitrogen partial pressure, where the value of E_g was found to decrease from 2.2 eV to 1.45 eV with the increasing NPP (nitrogen content) from 0% to 76.1% (0 at. % to 15.1 at.%). The value of E_g in a-C:H:N films strongly depend on sp^2 clusters size and the bonding. The nitrogen incorporation in a-C:H:N films takes place at the expense of carbon from C-C bonding, which promotes the formation of sp^2 bonding[19] and reduces E_g. Within the cluster model[20] the value of E_g in amorphous carbon depends on six fold rings in the clusters and can be estimated from $E_g = 2\gamma/M^{1/2}$, where γ is the nearest neighbour π interaction and M is the number of six-fold rings in the clusters. Thus, an increase in the size of six-fold π bonded sp^2 clusters embedded in amorphous sp^3 matrix reduces E_g of amorphous carbon films.

F. Temperature Dependent Conductivity Analysis

The electrical transport of a-C:H:N films strongly depends on the sp^2 bonding, where π-π^* states lie inside σ-σ^* states and control the conduction of charge carriers. Figure 7a shows the variation of conductivity (dark conductivity, DC and photoconductivity, PC) with inverse temperature for various a-C:H:N films. Here the conductivity was found to increase with increasing temperature

consistent with semiconducting behaviour. At zero nitrogen incorporation (sample S-1), the DC varied from ~ 4.6 x 10^{-11} to 2.7 x 10^{-9} $\Omega^{-1}cm^{-1}$ when the temperature was raised from 303 K to 473 K. However, no PC was observed in this film as light-generated electron-hole pairs readily recombine due to the low mobility of charge carriers. The magnitude of conductivity (both DC and PC) was enhanced as the nitrogen content increased. At low or zero nitrogen content, the concentration of sp^2 clusters is small and they are distributed in a random manner with a large separation between neighbouring clusters in an a-C:H matrix. The large separation between clusters reduces transport by hopping, resulting in low DC and no PC and explains why sample S-1 with a large band gap of 2.2 eV exhibits low DC and no PC. However, at higher nitrogen content, the concentration and size of sp^2 clusters in amorphous a-C:H matrix increases and the separation between the clusters reduces[24], this lowers the band gap, increasing the DC and PC. This explains why sample S-4 with 15.1 at.% nitrogen content with a lower band gap of 1.45 eV shows high DC and maximum PC.

In these films PC was only observed at lower temperatures because at higher temperatures the magnitude of DC itself swamped the PC signal. Recently, Umeno and Adhikari[21] have examined the conductivity of a-C:H:N films under dark and light conditions but photoconductivity only observed in their study at low temperatures with a PC/DC ratio (~ 1.2) at room temperature. Liu *et al.*[22] have explored the electrical properties of nitrogen incorporated ta-C (ta-C:N) films and found only a small photoconductivity with maximum PC/DC ratio ~ 1.03. Somani *et al.*[23] have studied the electrical conductivity of a-C:H:N films under dark and light (AM 1.5) conditions. They have found very weak photovoltaic effect even when they reduced the thickness of a-C:H:N films. We obtained maximum PC/DC ratio ~ 1.5 at room temperature in sample S-4. Hence, in view of the observed photoconductivity in our films grown at high pressure seems to be very encouraging and these a-C:H:N films could be employed in photovoltaic applications.

The activation energy (ΔE) for conduction is a very important electrical parameter to understand the transport mechanism. An Arrhenius plot of conductivity with temperature for each of these a-C:H:N films reveals two slopes: one in the lower temperature range and another in the higher temperature range, which infers the two modes of conduction with two activation energies ΔE_1 and ΔE_2. Therefore, the resultant conductivity is given by

$$\sigma = \sigma_{01} \exp(-\Delta E_1/ kT) + \sigma_{02} \exp(-\Delta E_2/kT), \quad (2)$$

where σ_{01} and σ_{02} are conductivity prefactors, k is Boltzmann's constant and T is the temperature in Kelvin. Figure 7b shows the variation of activation energy (ΔE_1 and ΔE_2) of DC and PC with nitrogen partial pressures. Since the slope was found to be smaller (larger) in the lower (higher) temperature range, the first (second) term of eq. (2) is dominant and the conductivity is governed by the activation energy ΔE_1 (ΔE_2). The behaviour of the activation energy is discussed in terms of band structure (Fig. 8). We interpret ΔE as the energy difference between the E_F and the conducting states. In disordered semiconductors, several localized states exist near the Fermi level as well as in the band tails. These semiconductors also contain extended states and the activation energy directly reflects the type of conduction. In the low temperature regime where the activation energy is found to be comparatively lower (ΔE_1) in the range 0.14 - 0.26 eV, the conduction takes place in localized states, situated at or very close to the Fermi level. However, at higher temperature regime where activation energy is found to be higher (ΔE_2) in the range 0.28 - 0.35 eV, the conduction occur either through states situated in the band tails or through extended states. Silva *et al.*[2] have also obtained same behaviour of activation energy in low and high temperature regimes. They have found ΔE between 0.34 eV and 0.55 eV in low temperature regime. In our case, the smaller activation energy in the lower and higher temperature regimes may be attributed to presence of large number of sp^2 clusters separated by a narrower gap due to which electrons

easily hope between the two successive clusters due to nitrogen incorporation. In addition, following important points should be kept in mind:

(i) Nitrogen may act as an n-type dopant for a-C:H films and its incorporation shifts the Fermi level (E_F) towards the conduction band.

(ii) As-deposited amorphous carbon films show weakly p-type behaviour as E_F in these films lie slightly below the mid gap [3]

(iii) Since disorder semiconductor (such as a-C:H or a-C:H:N) contains several states near the Fermi level as well as in band tails as suggested elsewhere,[20,24] the introduction of nitrogen in a-C:H:N films may be altered (increase or decrease) the size and concentration of these sp^2 states.

The activation energy may also be modified either due to the shifting of the Fermi level or due to the modification of the states. We schematically propose a model, shown in Fig. 8, where Fermi level is initially situated slightly below the mid-gap level for a-C:H:N film at zero nitrogen content but gets shifted towards conduction band with an increase of nitrogen content. The value of ΔE_1 and ΔE_2 (DC) for a-C:H:N film grown at NPP of 0% (sample S-1 or pure a-C:H film) was found to be 0.26 eV and 0.352 eV, respectively. This decreased to 0.142 eV and 0.348 eV, respectively, for a-C:H:N film deposited at NPP of 44.4% (sample S-2). With the increase of NPP from 0% to 44.4%, E_F shifts towards the conduction band and the energy difference between E_F and the conducting states is reduced, which results in reduced activation energies. The activation energies ΔE_1 and ΔE_2 (DC) for a-C:H:N film grown at NPP of 66.6% (sample S-3) are found to be 0.17 eV and 0.28 eV, respectively. In sample S-3, ΔE_1 is found to be lower than in sample S-1 but higher than ΔE_1 of sample S-2. On the other hand, ΔE_2 is lower in both samples S-1 and S-2. It was expected that at this NPP, E_F has shifted such that the carriers need only ~ 0.17 eV from E_F to conduct through either tunneling or hopping in localized states near Fermi level in low

temperature regime and they need 0.28 eV to conduct through jumping in band tail states or through the extended states. The values of ΔE_1 and ΔE_2 (DC) for a-C:H:N film grown at NPP of 76.1% (sample S-4) are found to be 0.19 eV and 0.32 eV, respectively, which were highest among nitrogen incorporated a-C:H:N films (among samples S-2, S-3 and S-4). We believe that conduction at higher temperature is due to hopping in band tail states.

We have also estimated the ΔE_1 and ΔE_2 from photoconductivity (PC) versus inverse of temperature plots. The ΔE_1 and ΔE_2 (PC) were found to be 0.26 eV and 0.36 eV for sample S-1, 0.147 eV and 0.362 eV for sample S-2, 0.142 eV and 0.281 eV for sample S-3, and 0.123 eV and 0.308 eV for sample S-4. Here, the cause of modification of activation energy for different samples was not only the shifting of Fermi level and a change to the electronic states with the introduction of nitrogen but also the change of states under exposure of light of intensity 100 mW/cm^2. The DC and PC of a-C:H:N films were also correlated with Tauc band gap, which is shown in Fig. 9. The DC and PC both varied inversely with band gap, i.e. lower the band gap greater the DC and PC. This may be due to the fact that low band gap was obtained at higher NPPs, and higher NPPs not only shifted the Fermi level towards the conduction band but also enhanced the conducting sp^2 bonding.

G. Analysis of the Electrical Characteristics of a-C:H:N/p-Si Devices

The current-voltage (I-V) characteristics of different a-C:H:N/p-Si heterojunction diodes in a sandwich structure configuration, where Al dots of diameter 1 mm are used as a metal contacts on a-C:H:N as well as on p-Si, were recorded and shown in Fig. 10a. These I-V curves clearly revealed the nonlinear behaviour and hence, the creation of rectifying circuits in the heterojunction has been realized. Furthermore, with the increasing nitrogen content not only does the current increases but also the diode turn-on voltage (V_{on}) decreases. In sample S-1 (NPP 0%), V_{on} was

found to be ~3 V, which shifted to ~ 2.5 V in sample S-2 (NPP 44.4%). In samples S-3 (NPP 66.6%) and S-4 (NPP 76.1%) again V_{on} shifted towards lower values and attained the magnitude as ~ 2 V and ~ 1.5 V, respectively. The plots of log I versus V for different a-C:H:N films revealed two different modes of conduction in which at higher voltage regime the curves were bent. Hence, I-V curves were fitted for log current versus voltage$^{1/2}$ (log I versus $V^{1/2}$), which as shown in Fig. 10b, to analyze electron transport. The investigation suggests that transport is bulk limited, not ruled by differences at the barrier heights at the contact. Therefore, occurrence of Poole-Frenkel model at higher voltage was realized, i.e. the conduction at higher voltage (or field) regime took place due to carriers trapped in the localized states. Recently, we have also observed Poole-Frenkel mechanism in a low pressure grown a-C:H:N/p-Si and a-C:H/n-Si heterojunction diodes[5]. Khan *et al.*[25] have found the Poole-Frenkel behaviour in low mass implanted amorphous carbon films and Miyajima *et al.*[26] have reported the Poole-Frenkel mechanism in pulse laser deposited nitrogen incorporated amorphous carbon films.

IV. CONCLUSIONS

The a-C:H:N films were deposited under various NPPs from 0% to 76.1% using RF-PECVD technique and were studied for their electrical, optical, mechanical and structural properties. The introduction of nitrogen in these films enhanced the graphite-like sp^2 bonding that was confirmed by XPS, FTIR and micro Raman analyses. The increase in nitrogen content or NPP reduced the residual stress, tuned the Tauc band gap towards lower values and improved the conductivity of these films with a reduction in hardness. Photoconductivity has also been observed in these films. An enhanced conductivity with increasing nitrogen content was discussed within a band model that revealed the shifting of Fermi level towards conduction band. The I-V characteristics clearly reveal the rectifying behaviour and their current continuously enhanced with increasing nitrogen

content. Analysis of the electrical characteristics also infers that electrical transport at higher voltages (or fields) in these films follow the Poole-Frenkel transport mechanism. Finally, observed excellent properties in high pressure deposited a-C:H:N films are very encouraging and may enhance its industrials applications as the present process is simple, cost effective and produces high throughput.

ACKNOWLEDGEMENT

The authors are grateful to the Director, National Physical Laboratory, New Delhi (India) for his kind support and encouragement. We acknowledge Mr. Ishpal, Dr. O. S. Panwar and Mr. C. M. S. Rauthan for their kind support. Author ND acknowledges CSIR, Govt. of India for providing financial support through SRF fellowship.

REFERENCES

[1] A. Y. Liu, and M. L. Cohen, Science **245**, 841 (1989).

[2] S. R. P. Silva, J. Robertson, G. A. J. Amaratunga, B. Rafferty, L. M. Brown, J. Schwan, D. F. Franceschini, and G. Mariotto, J. Appl. Phys. **81**, 2626 (1997).

[3] J. Schwan, V. Batori, S. Ulrich, and H. Ehrhardt, J. Appl. Phys. **84**, 2071 (1998).

[4] C. Godet, N. M. J. Conway, J. E. Bouree, K. Bouamra, A. Grosman, and C. Ortega, J. Appl. Phys. **91**, 4154 (2002).

[5] N. Dwivedi, S. Kumar, and H. K. Malik, J. Appl. Phys. **11**, 014908 (2012).

[6] N. Dwivedi, S. Kumar, and H. K. Malik, ACS Appl. Mater. Interfaces **3**, 4268 (2011).

[7] V. S. Veerasamy, G. A. J. Amaratunga, J. S. Park, W. I. Milne, H. S. Mckenzie, and D. S. Mckenzie, Appl. Phys. Lett. **64**, 2297 (1994).

[8] K. M. Krishna, M. Umeno, Y. Nukaya, T. Soga, and T. Jimbo, Appl. Phys. Lett. **77**, 1472 (2000).

[9] N. Konofaos, E. Evangelou, and S. Logothetidis, J. Appl. Phys. **86**, 4634 (1999).

[10] X. Gao, X. Zhang, C. Wan, X. Zhang, L. Wu, and X. Tan, Appl. Phys. Lett. **97**, 212101 (2010).

[11] I. Lazar, and G. Lazar, J. Non-Cryst. Solids **352**, 2096 (2006).

[12] S. R. P. Silva, and J. D. Carey, Diamond Relat. Mater. **12**, 151 (2003).

[13] C. Ronning, U. Greismeier, M. Groos, H. C. Hofsass, R. G. Downing, and G. P. Lamaze, Diamond. Relat. Mater. **4**, 666 (1995).

[14] C. Godet, and J. P. Kleider, J. Mater. Sci.:Mater. Electron. **17**, 413 (2006).

[15] S. J. Henley, J. D. Carey, and S. R. P. Silva, Appl. Phys. Lett. **25**, 6236 (2004).

[16] S. Kumar, N. Dwivedi, C. M. S. Rauthan, and O. S. Panwar, Vacuum **84**, 882 (2010).

[17] C. D. Wagner, W. M. Riggs, L. E. Davis, J. F. Moulder, G. E. Muilenberg, *Handbook of X-ray photoelectron spectroscopy*, Perkin Elmer Corporation (1979).

[18] A. C. Ferrari, J. Robertson, Philos. Trans. R. Soc. Lond. **362**, 2477 (2004).

[19] F. L. Freire Jr, J. Non-Cryst. Solids **304**, 251 (2002).

[20] J. Robertson, Mater. Sci. Eng. R **37**, 129 (2002).

[21] M. Umeno, and S. Adhikary Diamond Relat. Mater. **14**, 1973 (2005).

[22] S. Liu, G. Wang, and Z. Wang, J. Non-Cryst. Sol. 353 (2007) 2796.

[23] P. R. Somani, A. Yoshida, R. A. Afre, S. Adhikari, T. Soga, and M. Umeno, Phys. Stat. Sol. (a) **203**, 1982 (2006).

[24] J. D. Carey, and S. R. P. Silva, Phys. Rev. B **70**, 235417 (2004).

[25] R. U. A. Khan, J. D. Carey, and S. R. P. Silva, Phys. Rev. B **63**, 121201(R) (2001).

[26] Y. Miyajima, S. J. Henley, G. Adamopoulos, V. Stolojan, E. G. Caurel, B. Drevillon, J. M. Shannon, and S. R. P. Silva, J. Appl. Phys. **105**, 073521 (2009).

Figure Captions

Figure 1 XPS core level spectra of (a) C 1s for sample S-1, (b) C 1s for sample S-4 and (c) N 1s for sample S-4.

Figure 2 ToF-SIMS depth profile of a-C:H:N film grown at NPP of 76.1 %.

Figure 3 Deconvolved visible (5124 nm) Raman spectra of sample (a) S-1 and (b) S-4.

Figure 4 FTIR spectra of a-C:H:N films grown at NPP of (a) 0 % and (b) 76.1 %.

Figure 5 Variation of (a) S, (b) *H* and (c) E with NPP for a-C:H:N films.

Figure 6 Variation of Tauc band gap with NPP for a-C:H:N films.

Figure 7 (a) Variation of conductivity (DC and PC) with inverse of temperature for a-C:H:N films. The filled symbols with black line represent DC and open symbols with red line represent PC. (b) Variation of activation energy (for DC and PC) for a-C:H:N films.

Figure 8 Proposed model, showing shifting of Fermi level towards conduction band with the increase of NPP. This model was sketched on the basis of observed variation in electrical and optical properties with the changing NPP of a-C:H:N films.

Figure 9 Variation of conductivity (DC and PC) at 303 K with Tauc band gap.

Figure 10 (a) I-V characteristics and (b) Poole-Frenkel model (log I versus $V^{1/2}$) of different a-C:H:N films.

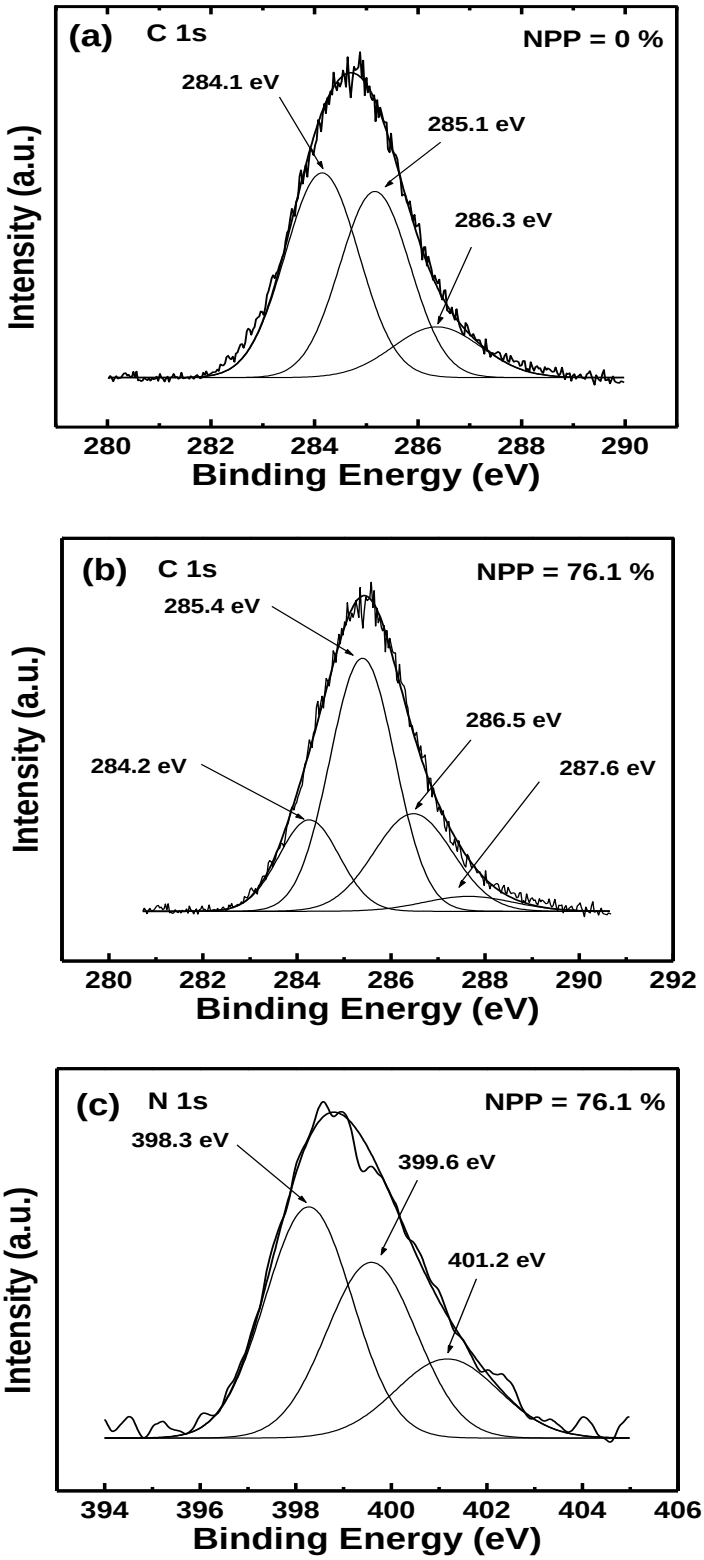
(a) C 1s
NPP = 0 %
284.1 eV
285.1 eV
286.3 eV
Intensity (a.u.)
280
282
284
286
288
290
Binding Energy (eV)
(b) C 1s
NPP = 76.1 %
285.4 eV
286.5 eV
284.2 eV
287.6 eV
Intensity (a.u.)
280
282
284
286
288
290
292
Binding Energy (eV)
(c) N 1s
NPP = 76.1 %
398.3 eV
399.6 eV
401.2 eV
Intensity (a.u.)
394
396
398
400
402
404
406
Binding Energy (eV)

Fig. 1

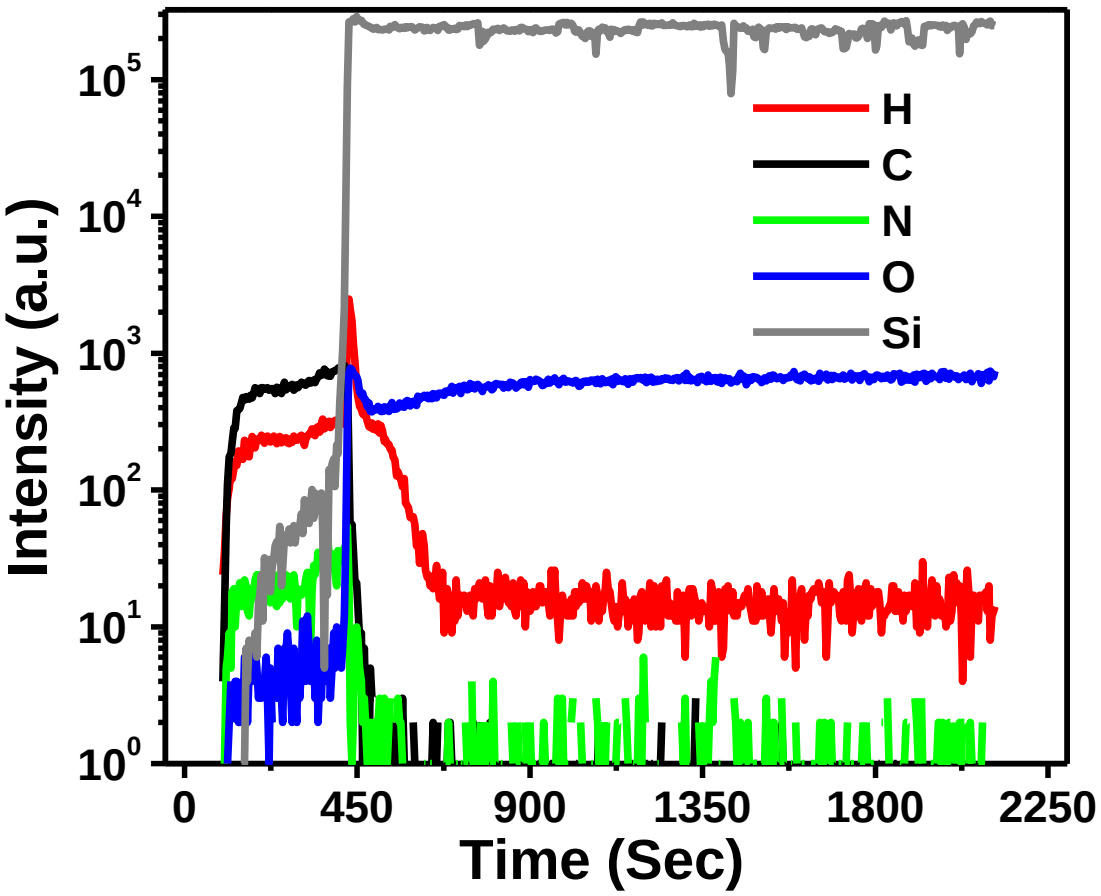
Intensity (a.u.)
10^0
10^1
10^2
10^3
10^4
10^5
0
450
900
1350
1800
2250
Time (Sec)
H
C
N
O
Si

Fig. 2

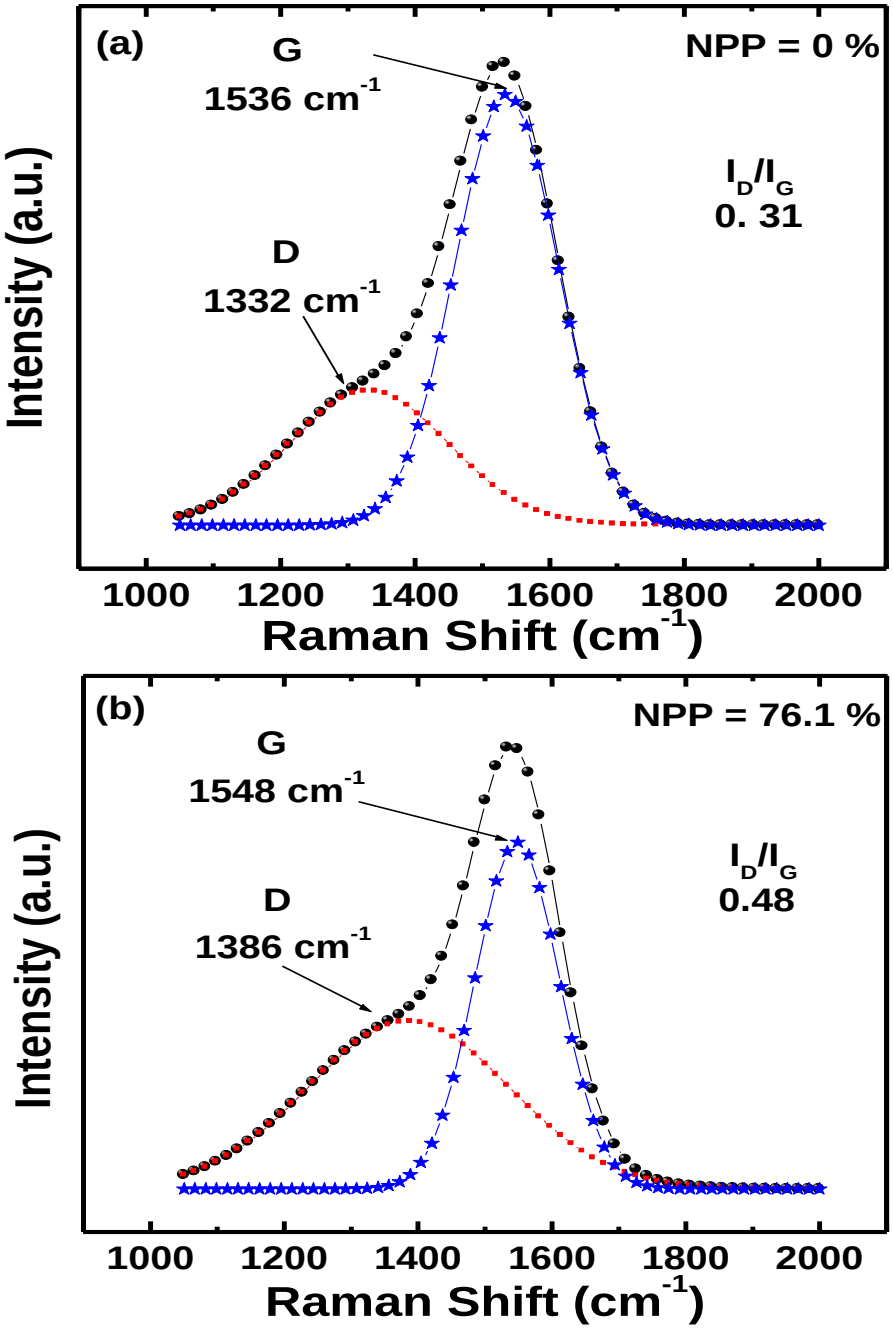
(a)
G
1536 cm-1
NPP = 0 %
ID/IG
0. 31
D
1332 cm-1
Intensity (a.u.)
1000
1200
1400
1600
1800
2000
Raman Shift (cm-1)
(b)
NPP = 76.1 %
G
1548 cm-1
ID/IG
0.48
D
1386 cm-1
Intensity (a.u.)
1000
1200
1400
1600
1800
2000
Raman Shift (cm-1)

Fig. 3

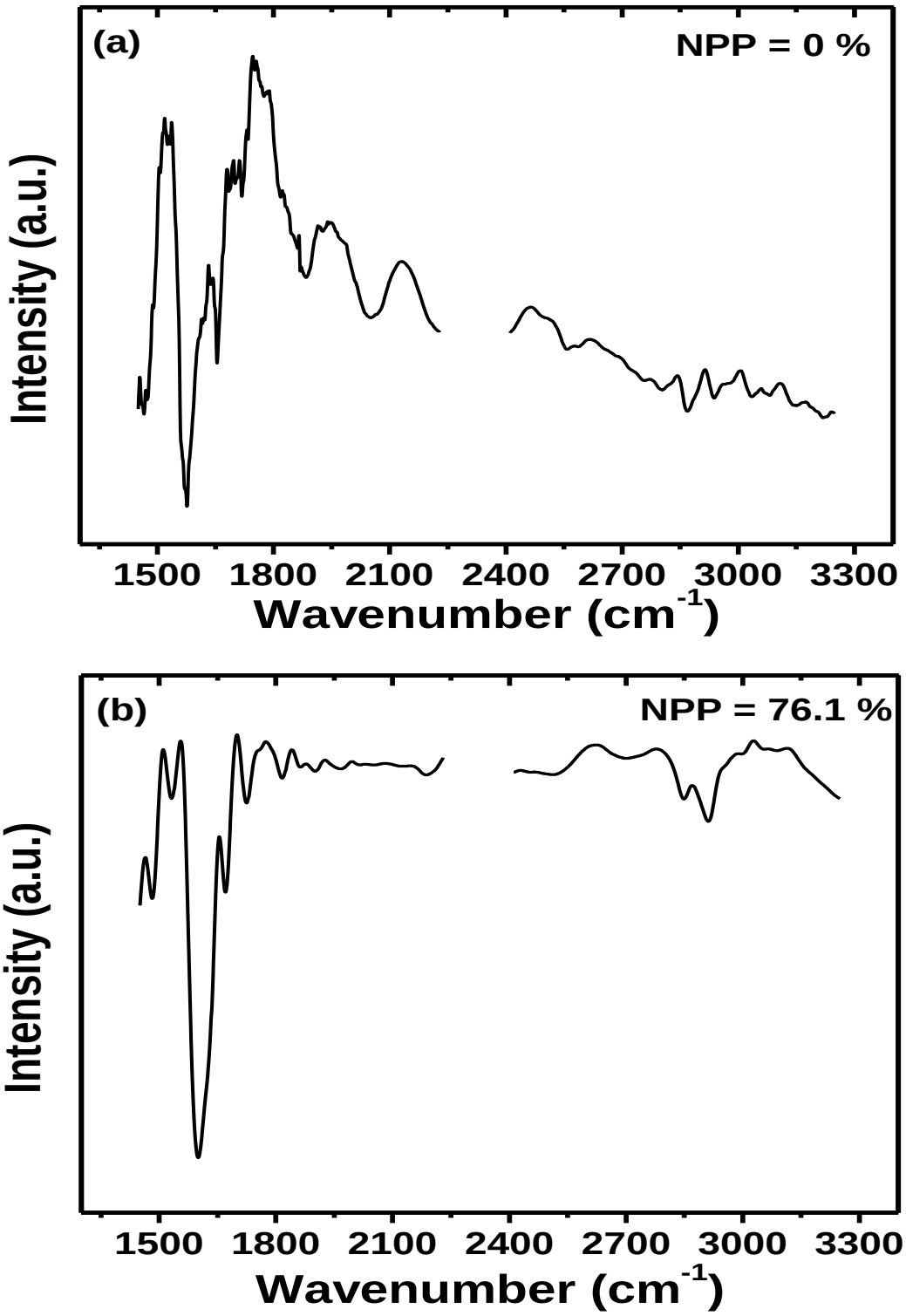
(a)
NPP = 0 %
Intensity (a.u.)
1500 1800 2100 2400 2700 3000 3300
Wavenumber (cm-1)
(b)
NPP = 76.1 %
Intensity (a.u.)
1500 1800 2100 2400 2700 3000 3300
Wavenumber (cm-1)

Fig. 4

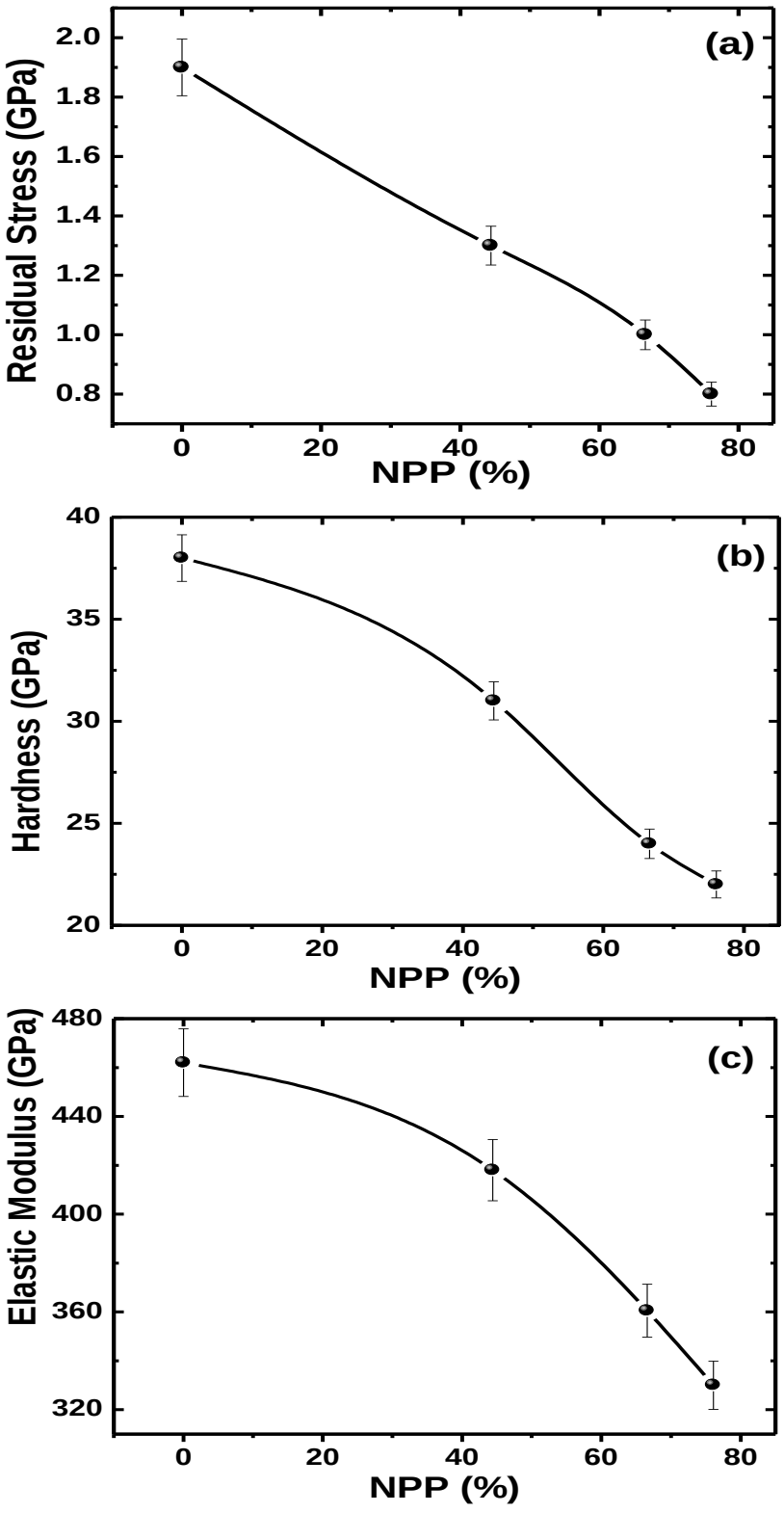
(a)
Residual Stress (GPa)
2.0
1.8
1.6
1.4
1.2
1.0
0.8
0
20
40
60
80
NPP (%)
(b)
Hardness (GPa)
40
35
30
25
20
0
20
40
60
80
NPP (%)
(c)
Elastic Modulus (GPa)
480
440
400
360
320
0
20
40
60
80
NPP (%)

Fig. 5

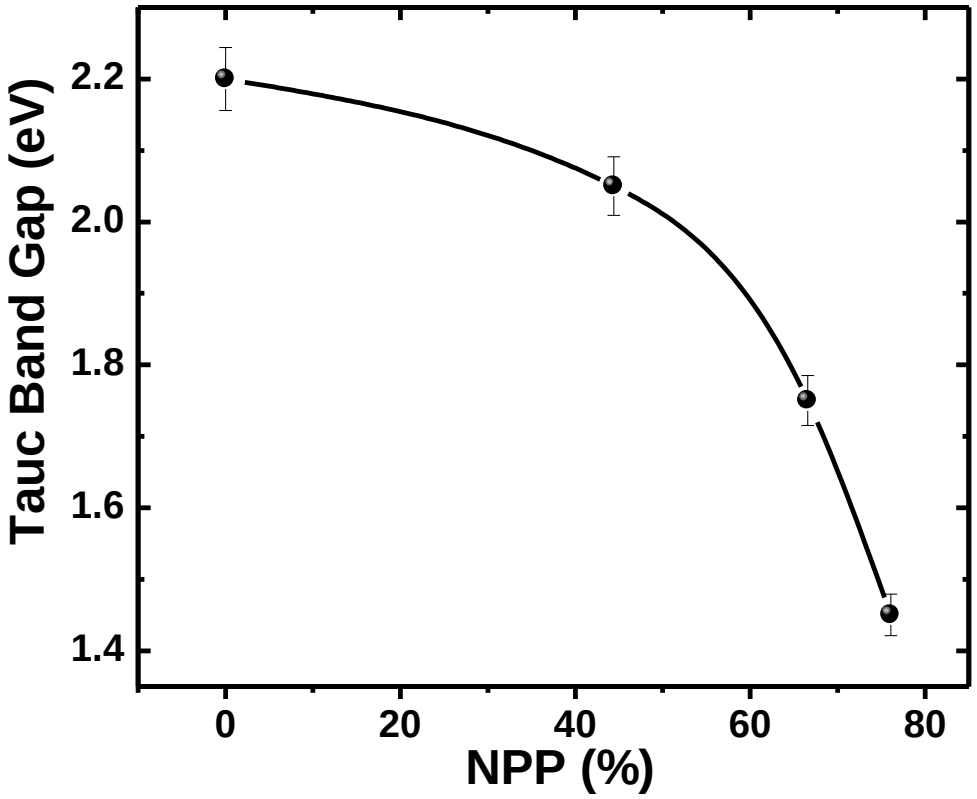

Fig. 6

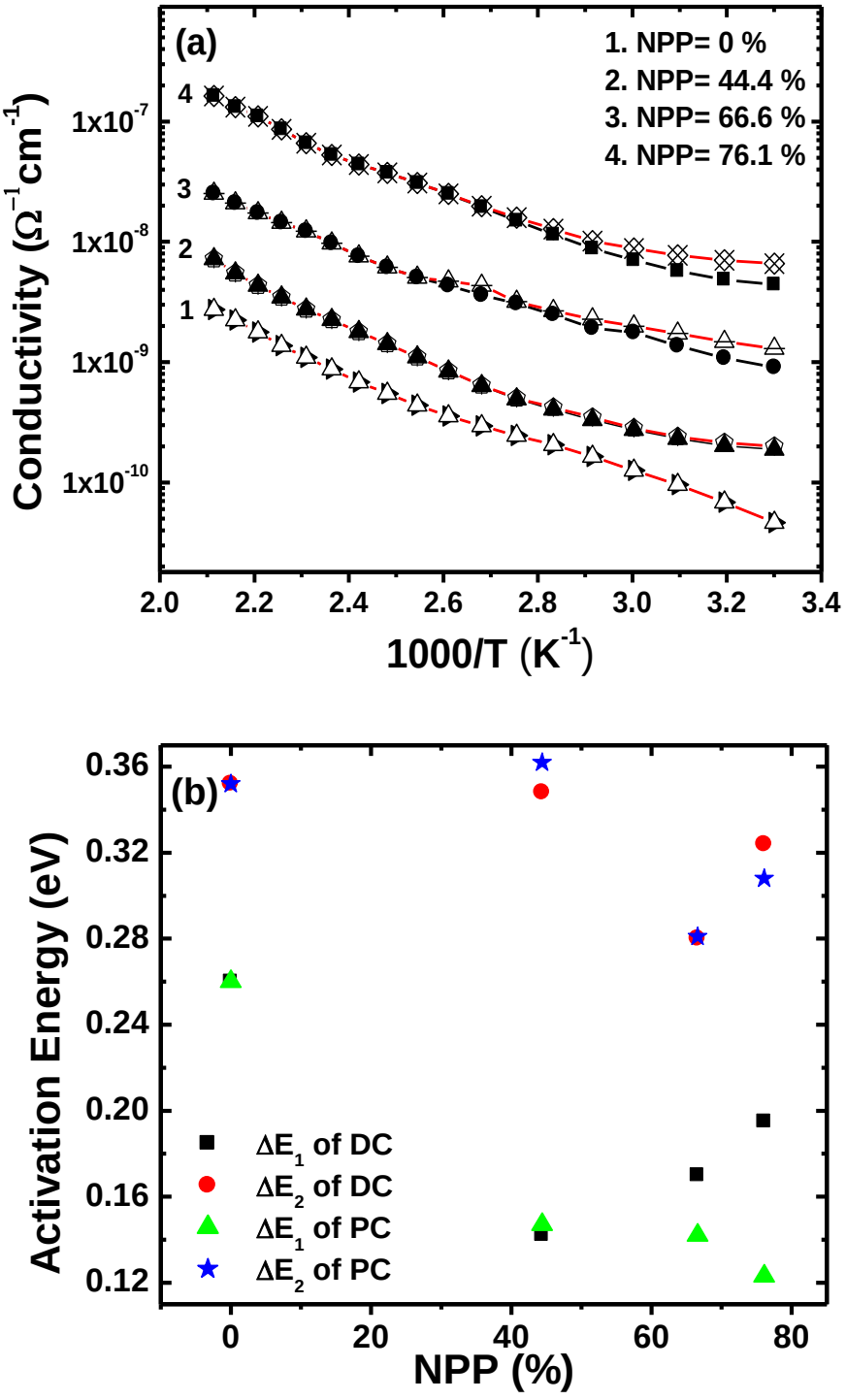
(a)
1. NPP= 0 %
2. NPP= 44.4 %
3. NPP= 66.6 %
4. NPP= 76.1 %
Conductivity (Ω⁻¹cm⁻¹)
1x10⁻⁷
1x10⁻⁸
1x10⁻⁹
1x10⁻¹⁰
1000/T (K⁻¹)
2.0
2.2
2.4
2.6
2.8
3.0
3.2
3.4
(b)
Activation Energy (eV)
0.36
0.32
0.28
0.24
0.20
0.16
0.12
ΔE1 of DC
ΔE2 of DC
ΔE1 of PC
ΔE2 of PC
0
20
40
60
80
NPP (%)

Fig. 7

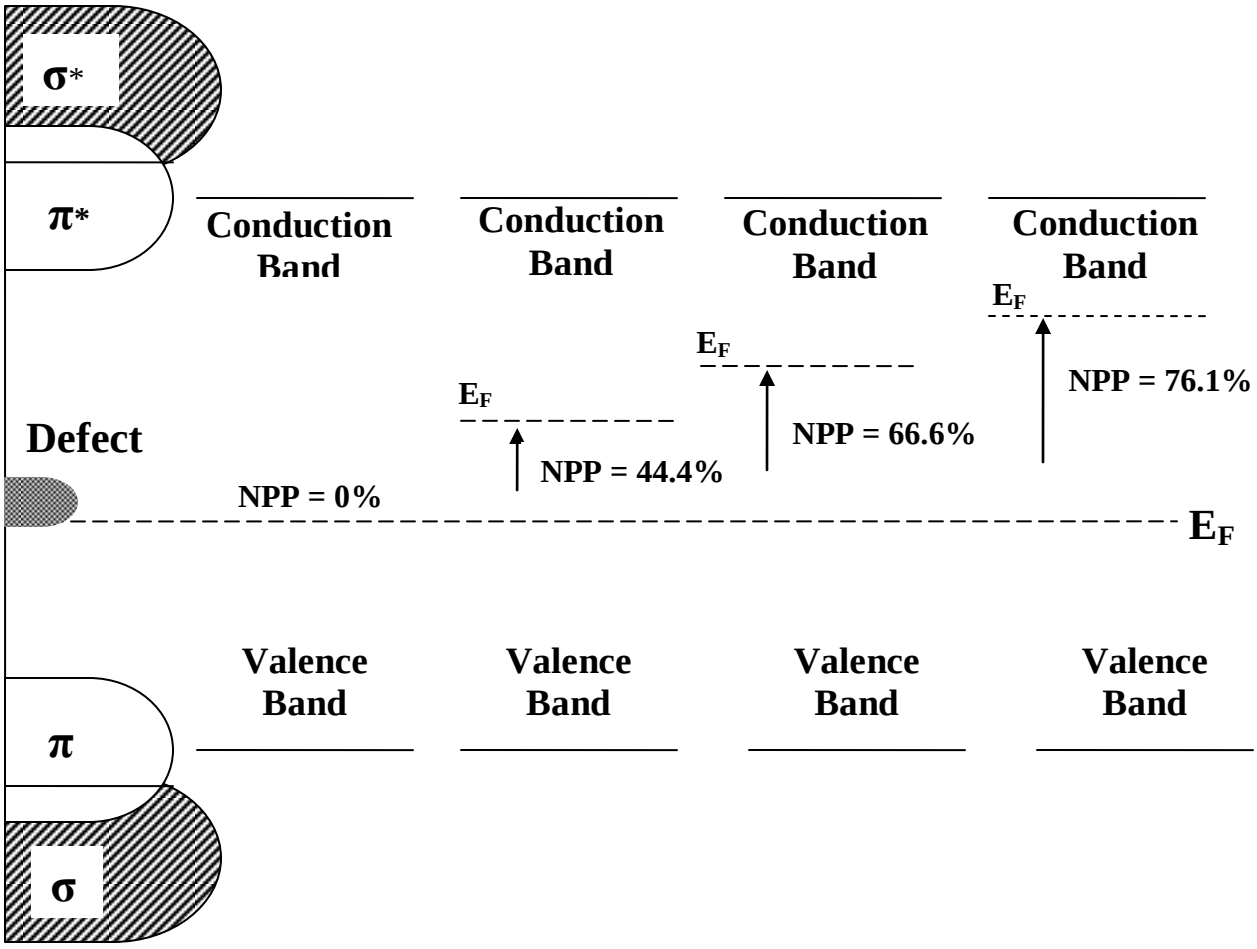
σ*
π*
Conduction Band
Conduction Band
Conduction Band
Conduction Band
E_F
E_F
E_F
NPP = 76.1%
NPP = 66.6%
NPP = 44.4%
Defect
NPP = 0%
E_F
Valence Band
Valence Band
Valence Band
Valence Band
π
σ

Fig. 8

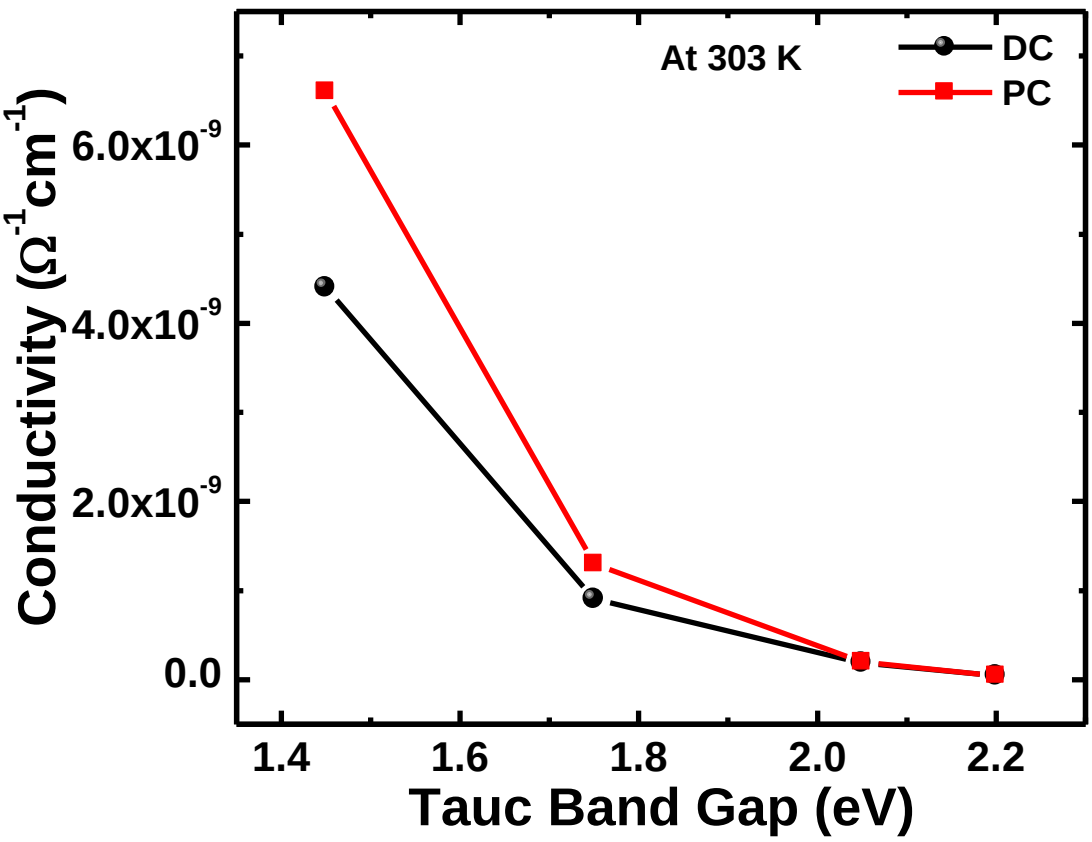
At 303 K
DC
PC
Conductivity (Ω-1cm-1)
6.0x10-9
4.0x10-9
2.0x10-9
0.0
1.4
1.6
1.8
2.0
2.2
Tauc Band Gap (eV)

Fig. 9

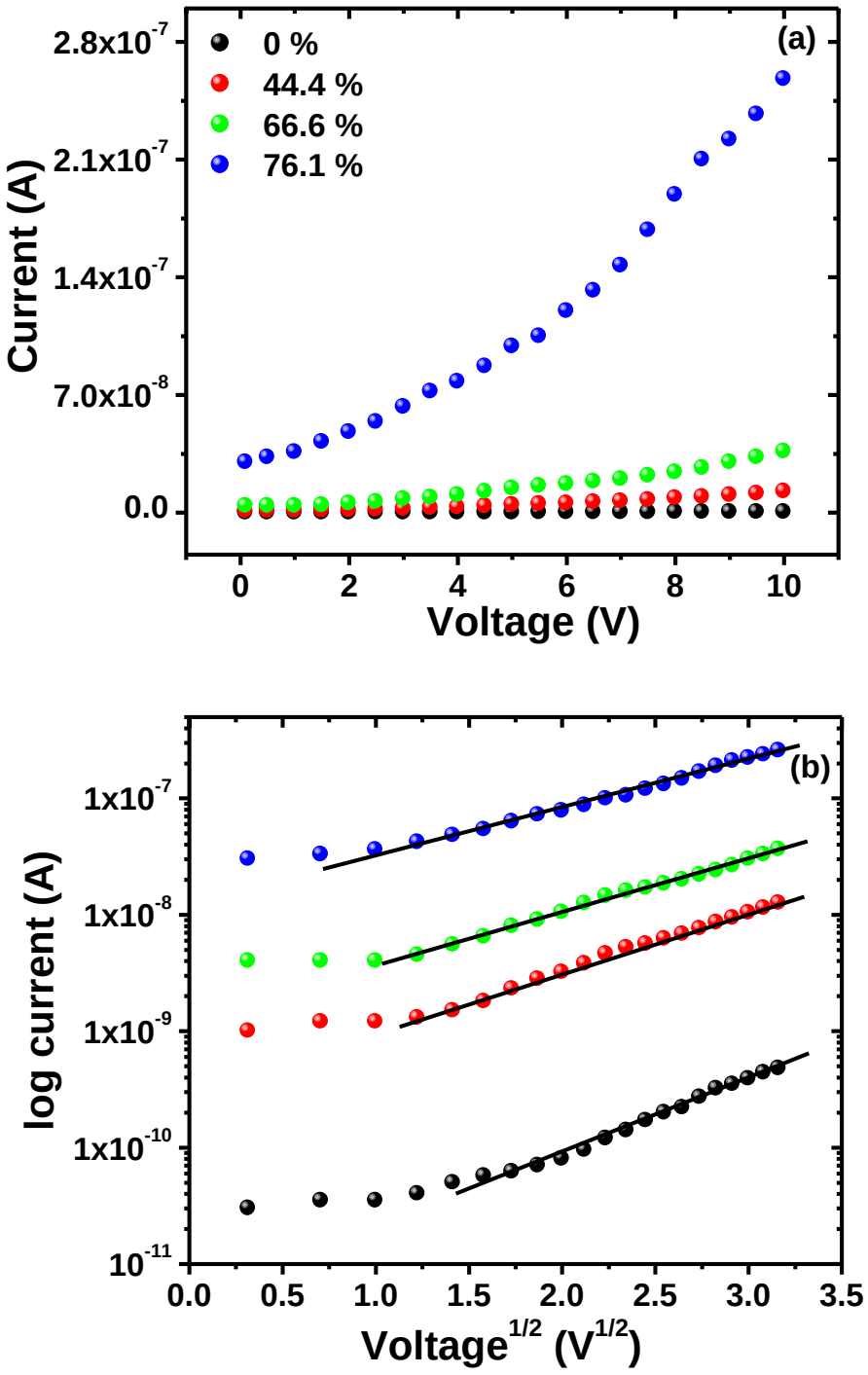
(a)
0 %
44.4 %
66.6 %
76.1 %
Current (A)
2.8x10-7
2.1x10-7
1.4x10-7
7.0x10-8
0.0
0
2
4
6
8
10
Voltage (V)
(b)
log current (A)
1x10-7
1x10-8
1x10-9
1x10-10
10-11
0.0
0.5
1.0
1.5
2.0
2.5
3.0
3.5
Voltage1/2 (V1/2)

Fig. 10